

Aberration-Aware Depth-from-Focus

Xinge Yang
KAUST
Saudi Arabia

xinge.yang@kaust.edu.sa

Qiang Fu
KAUST
Saudi Arabia

qiang.fu@kaust.edu.sa

Mohamed Elhoseiny
KAUST
Saudi Arabia

mohamed.elhoseiny@kaust.edu.sa

Wolfgang Heidrich
KAUST
Saudi Arabia

wolfgang.heidrich@kaust.edu.sa

Abstract

Computer vision methods for depth estimation usually use simple camera models with idealized optics. For modern machine learning approaches, this creates an issue when attempting to train deep networks with simulated data, especially for focus-sensitive tasks like Depth-from-Focus. In this work, we investigate the domain gap caused by off-axis aberrations that will affect the decision of the best-focused frame in a focal stack. We then explore bridging this domain gap through aberration-aware training (AAT). Our approach involves a lightweight network that models lens aberrations at different positions and focus distances, which is then integrated into the conventional network training pipeline. We evaluate the generality of pretrained models on both synthetic and real-world data. Our experimental results demonstrate that the proposed AAT scheme can improve depth estimation accuracy without fine-tuning the model or modifying the network architecture. Our code and models will be made publicly available.

1. Introduction

Modern deep-learning techniques have made significant progress in understanding 3D scenes from 2D RGB images, including depth estimation [24, 3, 43, 25], object detection [26, 47], multiple views [15, 39], and camera tracking and mapping [4, 34, 35]. However, these methods assume that 2D training images are aberration-free, relying on an idealized pinhole camera model that fails to account for out-of-focus effects and optical aberrations present in real camera lenses. This inaccuracy leads to a domain gap between experimental and real-world images, particularly given that modern lenses possess large apertures resulting in shallow depth-of-field (DoF), as well as a large field-of-view result-

ing in off-axis aberrations. The domain gap undermines the generalizability of trained deep learning models [9], necessitating engineers to fine-tune models with real data for each end device.

Recent studies in depth-from-focus (DfF) [33, 1, 5, 14, 30, 13, 22, 41, 42, 44] have recognized the impact of out-of-focus effects and explored using defocus cues for depth estimation and all-in-focus image prediction. DfF methods predict the probability that a pixel is the sharpest in a focal stack and then interpolate the input based on the probability, assuming that the sharpest frame is the best-focused frame. Although some of these methods [13, 22, 41, 42, 44] have claimed to bridge the domain gap between training and real-world images by considering that the sharpest pixel in the focal stack is independent of semantic information, their experiments have relied on a thin lens model that neglects off-axis optical aberrations commonly present in real lenses. Such aberrations, including field curvature, can cause the focus distance to vary across the image plane or result in asymmetric blurs that make it difficult to measure the most in-focus accurately frame. Moreover, studies [36, 6, 2, 21] have highlighted the impact of optical aberrations in depth estimation. Therefore, another domain gap arises due to the presence of optical aberrations.

To overcome the domain gap resulting from optical aberrations, we introduce aberration-aware training (AAT) to enable the network to learn these aberrations during training. Our AAT method consists of a lightweight point spread function (PSF) network and a re-rendering process to simulate aberrated training images. First, we compute the spatially-varying PSF of an optical lens using ray tracing [40, 46], and train a multilayer perceptron (MLP) to represent it. Once trained, the network can efficiently predict the PSF for different object positions and focus distances. Next, we render training images to apply off-axis aberrations.

tions. By randomly selecting focus distances and performing local convolution using all-in-focus images and their corresponding depth map, we create a focal stack containing depth-of-field and off-axis aberrations. After training the depth estimation network, the network learns to determine the best-focused frame for each pixel under optical aberrations, thereby enhancing the generalizability of pre-trained models. The depth estimation accuracy can be improved as long as the training and testing images are captured/simulated using the same lens.

To assess the effectiveness of our proposed AAT scheme, we conduct experiments to test the generalizability of the pre-trained DfF model on various datasets, including both simulated and real-world datasets. First, we simulate focal stacks using a real lens and a thin lens and train the corresponding DfF models. Then we test two models on focal stacks simulated/captured with the same lens without fine-tuning. The experimental results demonstrate that the AAT model generalizes better than the non-AAT model in terms of depth estimation accuracy. Specifically, the AAT model successfully resolves small depth differences between adjacent objects, whereas the non-AAT model fails to do so. Moreover, the AAT model proves more successful at suppressing the transfer of color texture detail into the depth geometry. Our training approach is agnostic to the specific DfF network architecture, and so we demonstrate results on two recent state-of-the-art architectures [44, 41].

In summary, our contributions are three-fold:

- We address the domain gap between simulated and real data arising from off-axis lens aberrations, which can significantly impact the determination of the best-focused frame in a focus stack and reduce the accuracy of depth estimation.
- We propose a lightweight network that can represent the PSF of a real lens for different object positions and focus distances. This PSF network can then be utilized to render realistic images for aberration-aware training.
- We propose an AAT scheme to bridge the domain gap between simulated and real-world data. Our experimental results demonstrate that DfF models trained with the AAT scheme can better generalize to test focal stacks captured or simulated using the same lens.

2. Related Works

2.1. Depth from Focus

Depth estimation is a fundamental task in computer vision, and can be tackled using different cues, such as semantic information [3, 25], stereo [11, 7, 28], and defocus [41, 44, 22]. Among these cues, the defocus cue is

considered domain invariant, as the defocus pattern is only related to the optical properties of the imaging lens. The depth-from-focus problem learns the depth map from the focus stack, using the idea that each pixel must have one frame that is best in focus.

Conventional approaches solve the depth-from-focus (DfF) problem as an optimization task [33, 32]. Learning-based approaches then use 2D convolutional neural networks (CNNs) to improve the accuracy of feature extraction and depth estimation [14, 5, 13, 22]. To allow for communication between different 2D CNNs, a shared pooling layer is used, and an intermediate defocus map [22] is learned during training to aid the depth estimation. Later, 3D CNNs [41, 42] started to replace 2D architectures, as they perform better in extracting shared information from an image stack. While the idea of the intermediate defocus map is kept, it is replaced by a 3D cost volume [41, 42, 44].

The training and testing datasets are obtained through various methods, including real-world captures and image simulation. For real-world captures, focal swap [33, 5] and light-field camera rendering [14] are two common methods used to obtain focused images, and additional Lidar or ToF cameras are used to get the depth map of the scene. Capturing real-world focal stacks with ground truth depth is quite expensive. Thus, image simulation methods, including PSF convolution [13], stereo image rendering [41], and software rendering [22], are also used to generate simulated focal stacks for training data augmentation. However, existing simulated focal stacks all rely on the idealized thin lens model and thus lack optical aberrations. Moreover, the real-world captured focal stacks lack focus distance information and lens data. In this work, we simulate aberrated focal stacks with the real lens model and capture real-world focal stacks with the necessary information. We use simulated focal stacks for training, and after training, we test the models on both simulated and real-world focal stacks without fine-tuning.

2.2. PSF Representation

The PSF is of great importance for image simulation, and multiple approaches have been introduced to calculate the PSF of an optical lens/system. Based on wave optics, a commonly used method involves propagating a point source spherical wave to the camera sensor through optical elements [12, 29]. Under this scenario, each optical element is treated as a phase plane that modulates the wavefront phase. Other methods calculate the PSF using paraxial optics [10, 13], and the result is a truncated Gaussian function called the “Circle-of-Confusion” (CoC). The diameter of the CoC is computed by

$$CoC = \frac{f}{N} \frac{|z - f_d|}{z} \frac{f}{f_d - f}, \quad (1)$$

where f_d is the focal distance, z is the distance between an object to the lens, f is the focal length, and N is the F-number of the camera lens. However, both methods yield simplified results due to the paraxial approximation, and therefore can not represent off-axis aberrations like field curvature, coma, and astigmatism in real optical lenses.

Ray tracing through optical lenses [17, 40] can provide a more accurate PSF and has been widely utilized in commercial software such as ZEMAX and CodeV. This method involves shooting rays from each object point source and calculating the distribution of each ray on the sensor plane to obtain the PSF. However, tracing rays through a sequence of optical elements is computationally expensive as it requires finding the intersection points of each ray using iterative algorithms. Recently, researchers have started exploring the use of neural networks to represent the PSF [38], which has shown promising results in both accuracy and speed. In this work, we follow this approach and propose a neural network-based method to represent the PSF for various positions and focus distances.

3. Methodology

As shown in Fig. 1(c), a classical DfF network takes the focus stack and corresponding focus distances as input and outputs a depth map. However, in the existing training pipeline, the focal stacks are pre-given and the network is blind to the optical system during training. Therefore, the pre-trained model is hard to generalize to real-world data, and computer vision engineers are required to fine-tune the model for better performance. With the idea of embedding optical knowledge into the network training, the AAT scheme integrates the data generation module into the network training pipeline, as illustrated in Fig. 1(b). All-in-focus images and their corresponding depth maps are used as input during training (Fig. 1(a)). A series of focus distances are then selected, and the PSF prediction network is applied to generate the PSF for each pixel, which is then used to render the focal stack. The entire pipeline can be executed end-to-end, and the AAT scheme allows the network to learn to predict depth maps in the presence of complex optical aberrations.

3.1. DfF Network

We do not modify the architecture of the DfF networks and instead use existing architectures such as AiFNet [41]. Given a batch of focal stacks with shapes (B, S, C, H, W), where B is the batch size, S is the number of images in the stack, C is the number of channels, and H, W are the image height and width, a 3D convolutional encoder is used to extract multilayer image features and create an intermediate attention map. This attention map is then used as an in-focus probability map to interpolate focus distances for the final depth prediction. The loss function for the DfF task

typically consists of a depth estimation loss and a regularization term:

$$L = L_{depth} + \omega L_{reg}, \quad (2)$$

where L_{depth} denotes the supervision loss function designed directly on the predicted depth map, and L_{reg} denotes the regularization term (e.g., one that encourages the depth map to be locally smooth using an edge-aware weighting as in [11]). ω is the weight coefficient balancing the two parts.

3.2. Aberration Simulator

Our contribution lies in the accurate simulation of aberrations for the training data to improve on the classical thin lens model. The PSF characterizes the optical lens response to a point source of light. We can convolve the per-pixel PSF with the object image to simulate the image captured by a camera. The Gaussian PSF assumes shift-invariance across the same depth. However, this simplified model does not accurately account for off-axis optical aberrations in a real imaging lens. In Fig. 2(b), we show the field curvature aberration, which is common in real lenses. Due to the field curvature, the pixel at the edge (P1) is blurry when the pixel on the axis (P2) is well-focused.

Ray tracing through optical lenses [17, 40] is widely used to obtain more accurate PSF. This involves tracing a group of rays from a point source to the sensor plane to generate a spot diagram. We can then compute the PSF by convolving the spot diagram with an energy distribution pattern and rasterizing it into sensor pixels [10, 16, 18]:

$$\text{PSF} = \sum_{k=1}^{spp} \mathbf{o}_k \cdot \delta_{i,j}(\mathbf{o}_k), \quad (3)$$

where \mathbf{o} is the intersection point of a ray with the sensor plane. $\delta_{i,j}$ denotes the energy distribution of a ray at pixel (i, j) . The term *spp*, short for “samples per pixel”, represents the number of rays emitted from each point source. In our experiments, we assume that the energy distribution of a ray is a unit impulse that equals zero except within the pixel. Since DfF is based on imaging with large apertures, it is possible to neglect diffraction effects which would dominate in optical systems with a small aperture. Moreover, we assume that chromatic aberrations are well corrected compared to the other aberrations and out-of-focus effects, which is the case for essentially all commercial-grade lenses. This allows us to simulate the optical system at a single wavelength of 550 nm.

However, ray tracing is computationally expensive, particularly as objects may appear at different positions and the focus distance may vary. Inspired by [38], we propose training a network H with parameters θ to represent the PSF as

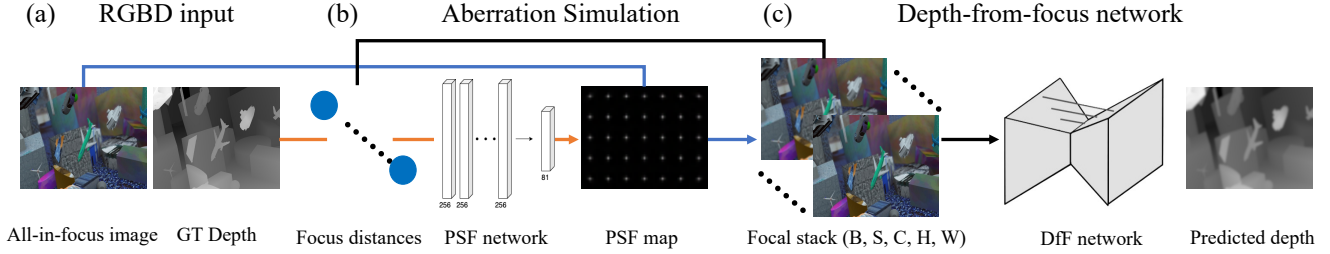


Figure 1. **Aberration-Aware Training pipeline.** (a) all-in-focus RGB images and corresponding depth maps are given as the input. (b) different focus distances are selected to simulate the focal swap process. The PSF network predicts PSF for different object positions and focus distances (orange pass). Then the PSF is convolved with the all-in-focus image to get the focal stack (blue pass). (c) the DfF network takes focal stack and focus distances to predict the depth map (black pass).

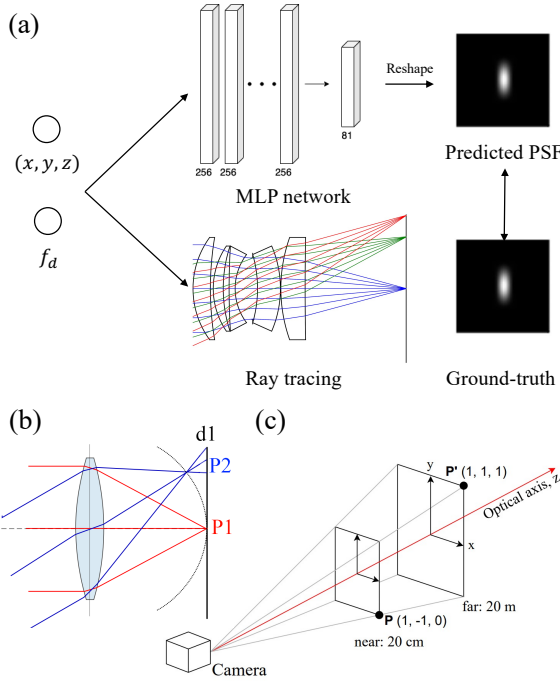


Figure 2. (a) a MLP network is trained to represent the PSF for different positions and focus distances. We use ray tracing to calculate accurate PSF as the ground truth. The network takes as input the object positions (x, y, z) and focus distance f_d , and produces a 2D matrix as output. (b) off-axis optical aberrations blur the pixels at the edge (P2) when the pixel on the axis (P1) is focused. (c) the valid imaging area is a frustum, and we normalize the x, y coordinates to $[-1, 1]$, z and f_d to $[0, 1]$.

$$\theta = \arg \min_{\theta} \|\text{PSF}(x, y, z; f_d) - H_{\theta}(x, y, z; f_d)\|_2^2, \quad (4)$$

where (x, y, z) represent the normalized coordinates of an object point, and f_d denotes the focus distance. As depicted in Fig. 2(a), we train the network H to fit an imaging lens by minimizing the difference between the predicted PSF and the ray-traced PSF. In object space, the valid imaging region

of a lens is a frustum (as shown in Fig. 2(c)) that is defined by the field of view (FoV), sensor size, minimum depth, and maximum depth. We then normalize the focus distance f_d and depth z to $[0, 1]$, and normalize (x, y) to $[-1, 1]$.

Once the optical structure and aperture size of a lens is fixed, the PSF is solely determined by the object position and focus distance. To map the four-parameter input into a 2D PSF kernel, we adopt a simple MLP network. The PSF prediction network consists of one input layer, five hidden layers with 256 neurons each, and an output layer with 81 neurons. We use ReLU activation functions after each input and hidden layer and a Sigmoid activation function after the output layer. The 81-channel output is then reshaped into a 9×9 2D tensor. After training, we fix the parameters of the PSF network and use it to predict the PSF for various object positions and focus distances. Then, we can use the per-pixel PSF to render aberrated images for the subsequent depth estimation task.

4. PSF Representation Results

4.1. Implementation Details

We train the PSF network for 400,000 iterations. In each iteration, we randomly focus the lens to a distance f_d , and select 64 points in object space for training. The ground-truth PSFs are computed by tracing 1024 rays from each object point, and input (x, y, z, f_d) is provided to the network for prediction. We simplify the problem by using a wavelength of 550 nm and a PSF size of 9×9 pixels. We use the AdamW optimizer [20] and CosineAnnealing learning rate scheduler [19] with default parameters. The initial learning rate is set to 1×10^{-3} . The lens has a minimum imaging depth of 20 cm and a maximum depth of 20 m, beyond which no relevant depth information can be recovered due to the small baseline of the DfF approach. We use the same depth range for the focus distance. We employ the DeepLens framework [40, 46] for ray tracing. The training process is run on a single A100 GPU and completed in approximately 6 hours. The network consists of 0.28 million

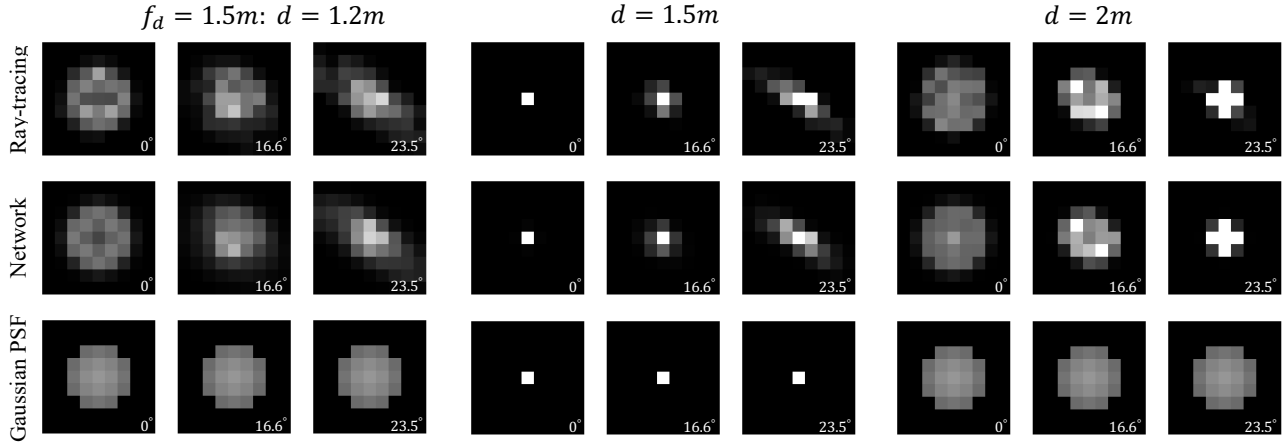


Figure 3. **PSF representation results.** We focus the lens to a distance of 1.5 m and evaluate the PSF of the three methods at three depths and three view angles. Our proposed PSF network produces a PSF that is similar to the ground truth (ray tracing). In contrast, the Gaussian PSF exhibits significant differences, particularly at large view angles. The PSF of a real lens varies with different view angles due to the presence of off-axis optical aberrations, while the Gaussian PSF model neglects this aberration.

parameters, with a storage size of approximately 1.5 MB.

4.2. Evaluation

We use the Canon EOS RF50mm F/1.8 lens for evaluation. The image sensor is simulated with physical dimensions of $24\text{mm} \times 32\text{mm}$ and a resolution of 640×960 to match the resolution of the RGBD data used for training the DfF network. While this image resolution is much lower than that of modern cameras, our experiments show that off-axis aberrations are still significant in the out-of-focus regime.

After training the PSF network, we focus the lens to a distance of 1.5 m and evaluate the PSF at depths of 1.2 m, 1.5 m, and 2 m, and three different view angles, as shown in Fig. 3. At the focused depth (1.5 m), the PSF is small, but when the lens is out of focus (1.2 m and 2 m), the PSF becomes larger. At 0° , both the network and the Gaussian model produced PSF that is close to the ground truth. However, as the view angle increases, the Gaussian PSF becomes increasingly inaccurate due to off-axis aberrations, and a clear difference is observed between the Gaussian PSF and the ground truth at 23.5° . In contrast, the PSF network predicts accurate results at all depths and view angles. Furthermore, at 23.5° , the ground truth PSF at a depth of 2 m is the smallest among the three depths, caused by optical aberrations (also illustrated in Fig. 2(b)). However, the Gaussian model can not capture this phenomenon. Comparing the network prediction and the ray tracing results, we find that the network-predicted PSF exhibits less noise and holds better symmetry, which is more in line with the physical situation.

In addition, we also compare our proposed network with the network developed by Tseng et al. [38] and present the quantitative results in Table 1. Specifically, we compared

Table 1. Quantitative results of our PSF network.

Method	ℓ_1 error	ℓ_2 error
Ours	$6.166e^{-3}$	$1.270e^{-4}$
Tseng, et, al. [38]	$1.000e^{-2}$	$3.463e^{-4}$

the ℓ_1 and ℓ_2 errors of the 11×11 predicted PSF across 37 depths and 37 focus distances. Our PSF network outperforms the network proposed by Tseng et al. in terms of accuracy. Furthermore, our PSF network takes discrete points and focus distances as input, whereas Tseng et al.’s network predict PSF grids at a certain depth. Consequently, our PSF network is more flexible to use, particularly for large amounts of varying points and focus distances.

5. Aberration-Aware Training Results

After evaluating the fitting quality of the PSF network, we now turn to evaluate the impact of using this network for aberration-aware training of the DfF network. To this end, we conduct experiments on both simulated and real-world data. First, we train and test the model on simulated focal stacks. Then, we train the model on simulated focal stacks and directly test it on real-world focal stacks. For the test data simulated/captured with a known lens, we simulate the training focal stacks with the same lens, as the AAT experiments.

For comparison, we simulate training focal stacks using the Gaussian PSF calculated with the thin lens model (“non-AAT”). This serves as the baseline, as used in the existing works. To ensure a fair comparison, the thin lens is set to have the same focal length, F-number, and sensor size as the real lens, with the only variable being the off-axis optical aberrations. For the experiments, we select two DfF networks: AiFNet [41] and DfVNet [44], and train them

Table 2. **Quantitative results on simulated focal stacks.** We choose two existing DfF networks, AiFNet [41] and DfVNet [44], and train two models for each network architecture. We then test these models on a new dataset without any fine-tuning. The pre-trained models demonstrate significant improvement with the AAT scheme.

Method	MAE ↓	MSE ↓	RMSE ↓	Abs. rel. ↓	Sqr. rel. ↓	$\delta = 1.25 \uparrow$	$\delta = 1.25^2 \uparrow$	$\delta = 1.25^3 \uparrow$
Baseline (AiFNet)	0.4706	0.4805	0.6229	0.2759	0.4906	0.8098	0.9587	0.9713
AAT (AiFNet)	0.2095	0.1536	0.3475	0.1613	0.2982	0.9683	0.9852	0.9895
Baseline (DfVNet)	0.5900	0.8452	0.8025	0.2885	0.5065	0.7390	0.8903	0.9277
AAT (DfVNet)	0.1977	0.1582	0.3446	0.1563	0.2992	0.9669	0.9830	0.9876

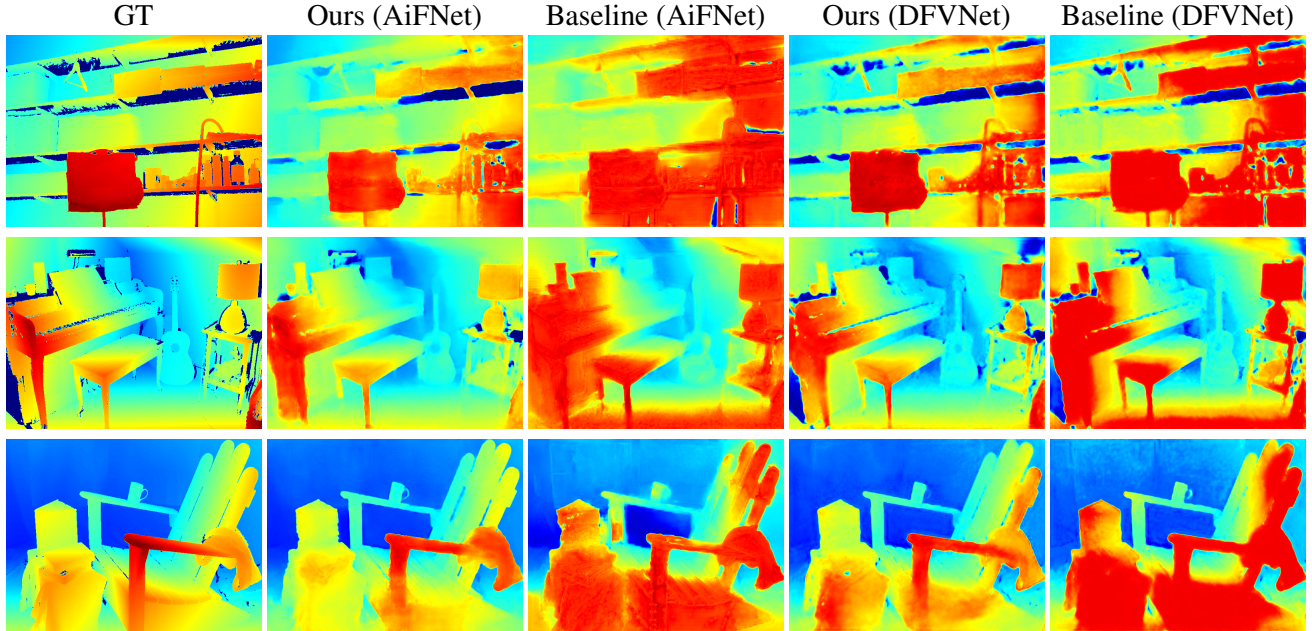


Figure 4. **Qualitative results on simulated focal stacks.** With the AAT scheme, both network models predict more accurate and finer depth maps, while the non-AAT models fail to distinguish between adjacent objects and also mispredict the depth of some edge objects.

with the same settings as described in the original papers. For each network, we train two models, one with the AAT scheme and one without it, and evaluate their performance on the testing focal stacks without any fine-tuning.

5.1. Implementation Details

In the simulation experiments, we use a 50mm F/2.8 lens¹ (see Fig.2(a)), which has more significant off-axis aberrations. The image sensor has a physical size of 24mm × 36mm and a resolution of 480 × 640, and we train a new PSF network to model this lens. The FlyingThings3D dataset [23, 41] is used as the training dataset, which contains 800 pairs of synthetic RGBD images. The Middlebury2014 dataset [27] is used as the testing dataset, which contains 23 real-world RGBD images. There is a significant domain gap between the synthetic and real-world images, making it suitable for evaluating the generalizability of the pre-trained DfF models. We simulate focal stacks with the RGBD images for training and testing, using a stack size of

10. The focus distances are chosen linearly from the minimum (20 cm) and maximum (20 m) depth range of each image, randomly perturbed.

We utilize the AdamW optimizer [20] and the CosineAnnealing learning rate scheduler [19] with their default parameters. The training batch size is 16, and the initial learning rate is $1e^{-4}$. Each DfF model is trained for 400 epochs on a single A100 GPU. Following training, we evaluate each model directly on the testing focal stacks without any fine-tuning.

In real-world experiments, we use the Canon EOS R camera and the RF 50mm F/1.8 lens discussed in Section 4. The training procedure keeps the same as the previous experiment. We use the Matterport3D dataset preprocessed by Zhang et al. [48], which comprises 117,516 pairs of indoor RGBD images as additional training data and train each model for an additional 20 epochs, followed by an evaluation of real-world captured focal stacks.

¹The lens data comes from lensnet.com [8]

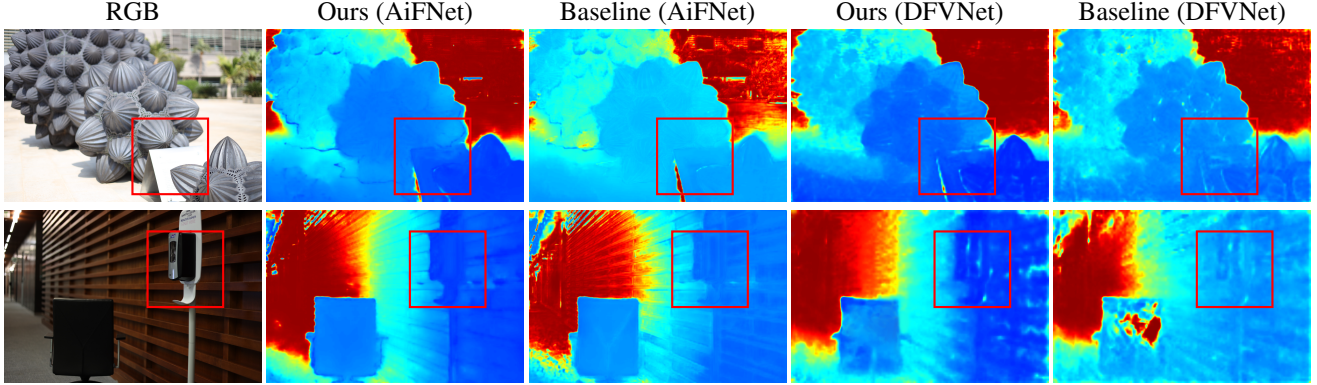


Figure 5. **Qualitative results on real-world outdoor focal stacks.** We capture real-world focal stacks using the same camera lens that is used for training and test pretrained models on them. The depth map predicted by AAT models is more hierarchical and can better distinguish depth differences between neighboring objects, as labeled by boxes.

5.2. Evaluation on Simulated Focal Stacks

In Fig. 4, we present the qualitative results of two DfF models with and without the AAT scheme. Both models predict promising depth maps with the AAT scheme, despite the significant domain gap between the original synthetic training data and the real-world test data. The AAT scheme effectively eliminates the domain gap since we simulate both training and testing focal stacks with the same lens model. We observe that small depth differences between adjacent objects are preserved in the predicted depth maps. Furthermore, the absolute depth values of the objects are precisely estimated without significant errors.

In comparison, the depth maps predicted by the non-AAT models fail to distinguish between adjacent objects, and also there are errors at the corner of the depth maps. This inaccuracy is caused by the off-axis aberrations, which is the only variable in the experiment. As illustrated in the previous section, the off-axis aberrations, such as field curvature, affects the decision of the best in-focus frame in the focus stack and degrade the performance of pre-trained models. These off-axis aberrations have a dominant effect at smaller out-of-focus depths, leading to the non-AAT model’s inability to discriminate between adjacent objects.

In Table. 2, we evaluate quantitative results with the following metrics: mean-absolute error (MAE), mean-squared error (MSE), root-mean-squared error (RMSE), log root-mean-squared error (logRMS), relative-absolute error (Abs.rel.), relative-squared error (Sqr.rel.), accuracy with $\delta = 1.25$. For MAE, MSE, RMSE, Abs.rel. and Sqr.rel., the lower the value, the better the results. And for three accuracies, the higher the value, the better the result. As shown in the table, both AiFNet and DFVNet models greatly improve with the AAT compared to the non-AAT results.

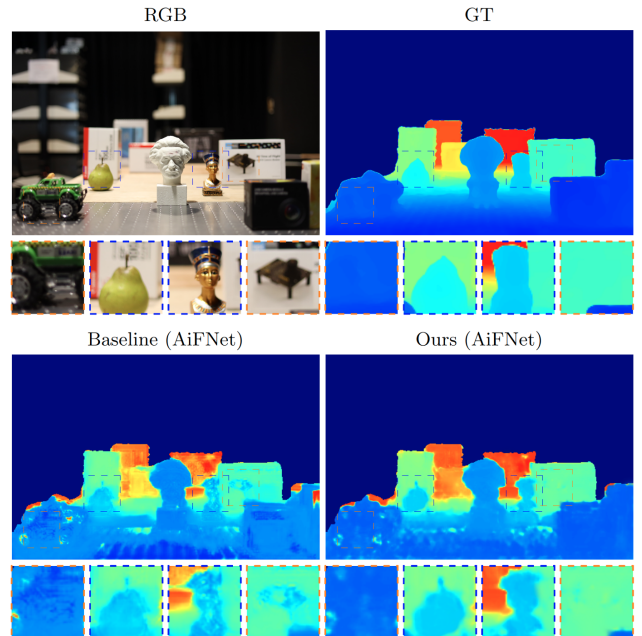


Figure 6. **Qualitative results on real-world indoor focal stacks.** We set up an indoor scene with objects placed at different positions. The non-AAT model incorrectly treats texture information in RGB images as depth information and also loses edge details in the predicted depth map.

Table 3. Quantitative results on real-world indoor focal stacks.

AiFNet [41]	MAE ↓	MSE ↓	Abs.Rel. ↓	$\delta = 1.25 \uparrow$
Baseline	0.1775	0.0836	0.1736	0.7978
Ours	0.1526	0.0770	0.1486	0.9029

5.3. Evaluation on Real-World Focal Stacks

We capture real-world focal stacks using the Canon RF 50 mm F/1.8 lens and test pre-trained DfF models. We select 24 outdoor scenes and one indoor scene for evaluation. The qualitative results of outdoor scenes are presented in

Fig.5, where we obtain the focus distance from the photo’s EXIF data. We observe that all models predict good depth maps, but the AAT-trained models provide finer details and smoother results. Moreover, the AAT-trained models give a more hierarchical depth map and can distinguish depth differences between neighboring objects better. In contrast, the non-AAT models predict less accurate depth maps, and the depth maps tend to confuse objects with little difference in depth, as indicated by the objects marked by boxes in the images. The two models exhibit significant differences at the corner of the predicted depth maps because off-axis lens aberrations are more pronounced at the image edge than at the center.

In Fig. 6, we present an indoor scene with objects at different positions and depths. We focus the camera on various objects to form the focal stack and measure more accurate focus distances with a ruler. Furthermore, we use the Lidar sensor from the iPhone14 Pro to scan the 3D scene, load the meshes into Blender software, and calibrate the camera’s position and view. After calibration, we render the depth map as the ground truth and calculate the score metrics. In Table. 3, the quantitative scores indicate that the AAT pre-trained model performs better than the baseline (“non-AAT”). We also observe from the zoomed image patches in Fig. 6 that the non-AAT model incorrectly treats texture information in RGB images as depth information and loses edge information. For more results on the real-world focal stacks, please refer to the Supplementary.

5.4. Training Time

We also analyze the extra time introduced by the AAT scheme, which results from the image re-rendering process. We use DFVNet to evaluate the training speed with varying numbers of stacks. In Fig.7, we report the average number of batches per second during training. For AAT, we render the focus stack for each batch during the training. For comparison, we render all focused images before the experiment and only load them to form focus stacks during the training. The average speed is calculated over 200 batches within a training epoch, and we run the model for 5 epochs to reduce the variance. When the stack size is small (≤ 4), the AAT training scheme reduces the training speed. However, in DfF applications, we typically use a stack size larger than 5 in our experiments, and the speed difference is negligible. Particularly, when the number of stacks is large (≥ 8), AAT training is faster due to the slower image reading process.

When the stack size equals 1, we analyze the additional time cost introduced in monocular image processing. The AAT scheme reduces the training speed by approximately 30%. However, this is also highly dependent on the network architecture. The DFVNet used for evaluation is a small and simple network; thus, the AAT scheme introduces a significant impact. However, we believe that this extra time can be

negligible for more complex and larger network structures.

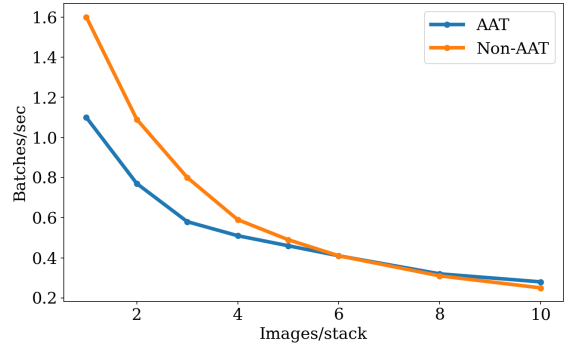


Figure 7. Comparison of training speed for different stack sizes.

6. Discussion

The experiments conducted in the previous section demonstrate that optical aberrations can degrade the generalizability of pretrained DfF models, but we can improve the results with the proposed AAT scheme. However, there are also some limitations that need to be considered, especially in real-world practice.

Firstly, the impact of optical aberrations is significant only for small defocus distances, as the PSF is dominated by defocus phenomena when object points are far from the focus plane. Therefore, the AAT scheme is more effective in improving depth estimation accuracy for adjacent objects with less significant defocus. However, in sparse scenes, the improvement may not be as significant.

Secondly, the AAT scheme can provide more significant improvement for lenses with more aberrations. For commercial cameras, the impact of the AAT scheme may be limited as optical designers correct the aberrations well. However, we believe that the AAT scheme will play a more important role in the context of end-to-end trained compact computational imaging lenses [31, 18, 37, 45] in the future.

Thirdly, the focus distance information obtained from the EXIF data of photography cameras is often inaccurate, leading to reduced depth estimation performance. However, modern imaging and display systems typically include Lidar or depth cameras that can provide more accurate focus distance information. By incorporating such information, we believe the depth estimation performance can be further improved, especially in scenarios where multiple cameras are employed.

7. Conclusion

In this work, we address the domain gap caused by off-axis optical aberrations, which has been overlooked by most existing works. To this end, we propose an AAT scheme to bridge this gap. Specifically, we develop a network to predict the PSF of a real camera lens for different positions and

focus distances. We then use the predicted PSF to simulate aberrated training images, enabling the network to learn to extract more accurate image features in the presence of optical aberrations. We evaluate the AAT scheme on two DfF networks and demonstrate its generalizability through both simulated and real-world experiments. The experimental results indicate that the AAT scheme improves the generalizability of the DfF models. The DfF models trained with AAT can predict more accurate depth maps without fine-tuning compared to the baseline. Furthermore, we believe that the AAT scheme is not limited to the DfF task and can be applied to improve the generalizability of other computer vision tasks.

References

- [1] Saeed Anwar, Zeeshan Hayder, and Fatih Porikli. Depth estimation and blur removal from a single out-of-focus image. In *BMVC*, volume 1, page 2, 2017. 1
- [2] Seung-Hwan Baek, Hayato Ikoma, Daniel S Jeon, Yuqi Li, Wolfgang Heidrich, Gordon Wetzstein, and Min H Kim. Single-shot hyperspectral-depth imaging with learned diffractive optics. In *Proceedings of the IEEE/CVF International Conference on Computer Vision*, pages 2651–2660, 2021. 1
- [3] Shariq Farooq Bhat, Ibraheem Alhashim, and Peter Wonka. Adabins: Depth estimation using adaptive bins. In *Proceedings of the IEEE/CVF Conference on Computer Vision and Pattern Recognition*, pages 4009–4018, 2021. 1, 2
- [4] Michael Bloesch, Jan Czarnowski, Ronald Clark, Stefan Leutenegger, and Andrew J Davison. Codeslam—learning a compact, optimisable representation for dense visual slam. In *Proceedings of the IEEE conference on computer vision and pattern recognition*, pages 2560–2568, 2018. 1
- [5] Marcela Carvalho, Bertrand Le Saux, Pauline Trouvé-Peloux, Andrés Almansa, and Frédéric Champagnat. Deep depth from defocus: how can defocus blur improve 3d estimation using dense neural networks? In *Proceedings of the European Conference on Computer Vision (ECCV) Workshops*, pages 0–0, 2018. 1, 2
- [6] Julie Chang and Gordon Wetzstein. Deep optics for monocular depth estimation and 3d object detection. In *Proceedings of the IEEE/CVF International Conference on Computer Vision*, pages 10193–10202, 2019. 1
- [7] Jia-Ren Chang and Yong-Sheng Chen. Pyramid stereo matching network. In *Proceedings of the IEEE conference on computer vision and pattern recognition*, pages 5410–5418, 2018. 2
- [8] Geoffroi Côté, Jean-François Lalonde, and Simon Thibault. Deep learning-enabled framework for automatic lens design starting point generation. *Optics express*, 29(3):3841–3854, 2021. 6
- [9] Jose M Facil, Benjamin Ummenhofer, Huizhong Zhou, Luis Montesano, Thomas Brox, and Javier Civera. Cam-convs: Camera-aware multi-scale convolutions for single-view depth. In *Proceedings of the IEEE/CVF Conference on Computer Vision and Pattern Recognition*, pages 11826–11835, 2019. 1
- [10] Michael Harold Freeman. *Optics*. Butterworth-Heinemann, 1990. 2, 3
- [11] Clément Godard, Oisín Mac Aodha, and Gabriel J Brostow. Unsupervised monocular depth estimation with left-right consistency. In *Proceedings of the IEEE conference on computer vision and pattern recognition*, pages 270–279, 2017. 2, 3
- [12] Joseph W Goodman. *Introduction to Fourier optics*. Roberts and Company publishers, 2005. 2
- [13] Shir Gur and Lior Wolf. Single image depth estimation trained via depth from defocus cues. In *Proceedings of the IEEE/CVF Conference on Computer Vision and Pattern Recognition*, pages 7683–7692, 2019. 1, 2
- [14] Caner Hazirbas, Sebastian Georg Soyer, Maximilian Christian Staab, Laura Leal-Taixé, and Daniel Cremers. Deep depth from focus. In *Asian conference on computer vision*, pages 525–541. Springer, 2018. 1, 2
- [15] Po-Han Huang, Kevin Matzen, Johannes Kopf, Narendra Ahuja, and Jia-Bin Huang. Deepmvs: Learning multi-view stereopsis. In *Proceedings of the IEEE Conference on Computer Vision and Pattern Recognition*, pages 2821–2830, 2018. 1
- [16] Francis Arthur Jenkins and Harvey Elliott White. Fundamentals of optics. *Indian Journal of Physics*, 25:265–266, 1957. 3
- [17] Craig Kolb, Don Mitchell, and Pat Hanrahan. A realistic camera model for computer graphics. In *Proceedings of the 22nd annual conference on computer graphics and interactive techniques*, pages 317–324, 1995. 3
- [18] Zongling Li, Qingyu Hou, Zhipeng Wang, Fanjiao Tan, Jin Liu, and Wei Zhang. End-to-end learned single lens design using fast differentiable ray tracing. *Optics Letters*, 46(21):5453–5456, 2021. 3, 8
- [19] Ilya Loshchilov and Frank Hutter. Sgdr: Stochastic gradient descent with warm restarts. *arXiv preprint arXiv:1608.03983*, 2016. 4, 6
- [20] Ilya Loshchilov and Frank Hutter. Decoupled weight decay regularization. *arXiv preprint arXiv:1711.05101*, 2017. 4, 6
- [21] Miguel Marquez, Pablo Meza, Fernando Rojas, Henry Arguello, and Esteban Vera. Snapshot compressive spectral depth imaging from coded aberrations. *Optics Express*, 29(6):8142–8159, 2021. 1
- [22] Maxim Maximov, Kevin Galim, and Laura Leal-Taixé. Focus on defocus: bridging the synthetic to real domain gap for depth estimation. In *Proceedings of the IEEE/CVF Conference on Computer Vision and Pattern Recognition*, pages 1071–1080, 2020. 1, 2
- [23] Nikolaus Mayer, Eddy Ilg, Philip Hausser, Philipp Fischer, Daniel Cremers, Alexey Dosovitskiy, and Thomas Brox. A large dataset to train convolutional networks for disparity, optical flow, and scene flow estimation. In *Proceedings of the IEEE conference on computer vision and pattern recognition*, pages 4040–4048, 2016. 6
- [24] Simon Niklaus, Long Mai, Jimei Yang, and Feng Liu. 3d ken burns effect from a single image. *ACM Transactions on Graphics (ToG)*, 38(6):1–15, 2019. 1

- [25] Vaishakh Patil, Christos Sakaridis, Alexander Liniger, and Luc Van Gool. P3depth: Monocular depth estimation with a piecewise planarity prior. In *Proceedings of the IEEE/CVF Conference on Computer Vision and Pattern Recognition*, pages 1610–1621, 2022. 1, 2
- [26] Joseph Redmon, Santosh Divvala, Ross Girshick, and Ali Farhadi. You only look once: Unified, real-time object detection. In *Proceedings of the IEEE conference on computer vision and pattern recognition*, pages 779–788, 2016. 1
- [27] Daniel Scharstein, Heiko Hirschmüller, York Kitajima, Greg Krathwohl, Nera Nešić, Xi Wang, and Porter Westling. High-resolution stereo datasets with subpixel-accurate ground truth. In *German conference on pattern recognition*, pages 31–42. Springer, 2014. 6
- [28] Zhelun Shen, Yuchao Dai, and Zhibo Rao. Cfnets: Cascade and fused cost volume for robust stereo matching. In *Proceedings of the IEEE/CVF Conference on Computer Vision and Pattern Recognition*, pages 13906–13915, 2021. 2
- [29] Vincent Sitzmann, Steven Diamond, Yifan Peng, Xiong Dun, Stephen Boyd, Wolfgang Heidrich, Felix Heide, and Gordon Wetzstein. End-to-end optimization of optics and image processing for achromatic extended depth of field and super-resolution imaging. *ACM Transactions on Graphics (TOG)*, 37(4):1–13, 2018. 2
- [30] Pratul P Srinivasan, Rahul Garg, Neal Wadhwa, Ren Ng, and Jonathan T Barron. Aperture supervision for monocular depth estimation. In *Proceedings of the IEEE Conference on Computer Vision and Pattern Recognition*, pages 6393–6401, 2018. 1
- [31] Qilin Sun, Congli Wang, Fu Qiang, Dun Xiong, and Heidrich Wolfgang. End-to-end complex lens design with differentiable ray tracing. *ACM Trans. Graph.*, 40(4):1–13, 2021. 8
- [32] Jaeheung Surh, Hae-Gon Jeon, Yunwon Park, Sunghoon Im, Hyowon Ha, and In So Kweon. Noise robust depth from focus using a ring difference filter. In *Proceedings of the IEEE Conference on Computer Vision and Pattern Recognition*, pages 6328–6337, 2017. 2
- [33] Supasorn Suwajanakorn, Carlos Hernandez, and Steven M Seitz. Depth from focus with your mobile phone. In *Proceedings of the IEEE Conference on Computer Vision and Pattern Recognition*, pages 3497–3506, 2015. 1, 2
- [34] Chengzhou Tang and Ping Tan. Ba-net: Dense bundle adjustment network. *arXiv preprint arXiv:1806.04807*, 2018. 1
- [35] Keisuke Tateno, Federico Tombari, Iro Laina, and Nassir Navab. CNN-SLAM: Real-time dense monocular slam with learned depth prediction. In *Proceedings of the IEEE conference on computer vision and pattern recognition*, pages 6243–6252, 2017. 1
- [36] Pauline Trounev, Frédéric Champagnat, Guy Le Besnerais, Jacques Sabater, Thierry Avignon, and Jérôme Idier. Passive depth estimation using chromatic aberration and a depth from defocus approach. *Applied optics*, 52(29):7152–7164, 2013. 1
- [37] Ethan Tseng, Shane Colburn, James Whitehead, Luocheng Huang, Seung-Hwan Baek, Arka Majumdar, and Felix Heide. Neural nano-optics for high-quality thin lens imaging. *Nature communications*, 12(1):6493, 2021. 8
- [38] Ethan Tseng, Ali Mosleh, Fahim Mannan, Karl St-Arnaud, Avinash Sharma, Yifan Peng, Alexander Braun, Derek Nowrouzezahrai, Jean-Francois Lalonde, and Felix Heide. Differentiable compound optics and processing pipeline optimization for end-to-end camera design. *ACM Transactions on Graphics (TOG)*, 40(2):1–19, 2021. 3, 5
- [39] Benjamin Ummenhofer, Huizhong Zhou, Jonas Uhrig, Nikolaus Mayer, Eddy Ilg, Alexey Dosovitskiy, and Thomas Brox. Demon: Depth and motion network for learning monocular stereo. In *Proceedings of the IEEE conference on computer vision and pattern recognition*, pages 5038–5047, 2017. 1
- [40] Congli Wang, Ni Chen, and Wolfgang Heidrich. dO: A differentiable engine for deep lens design of computational imaging systems. *IEEE Transactions on Computational Imaging*, 8:905–916, 2022. 1, 3, 4
- [41] Ning-Hsu Wang, Ren Wang, Yu-Lun Liu, Yu-Hao Huang, Yu-Lin Chang, Chia-Ping Chen, and Kevin Jou. Bridging unsupervised and supervised depth from focus via all-in-focus supervision. In *Proceedings of the IEEE/CVF International Conference on Computer Vision*, pages 12621–12631, 2021. 1, 2, 3, 5, 6, 7
- [42] Changyeon Won and Hae-Gon Jeon. Learning depth from focus in the wild. In *European Conference on Computer Vision*, pages 1–18. Springer, 2022. 1, 2
- [43] Zhenda Xie, Zigang Geng, Jingcheng Hu, Zheng Zhang, Han Hu, and Yue Cao. Revealing the dark secrets of masked image modeling. *arXiv preprint arXiv:2205.13543*, 2022. 1
- [44] Fengting Yang, Xiaolei Huang, and Zihan Zhou. Deep depth from focus with differential focus volume. In *Proceedings of the IEEE/CVF Conference on Computer Vision and Pattern Recognition*, pages 12642–12651, 2022. 1, 2, 5, 6
- [45] Xinge Yang, Qiang Fu, and Wolfgang Heidrich. Automatic lens design based on differentiable ray-tracing. In *Imaging and Applied Optics Congress 2022 (3D, AOA, COSI, ISA, pcAOP)*, page CTh4C.2. Optica Publishing Group, 2022. 8
- [46] Xinge Yang, Qiang Fu, and Wolfgang Heidrich. Curriculum learning for ab initio deep learned refractive optics. *arXiv preprint arXiv:2302.01089*, 2023. 1, 4
- [47] Hao Zhang, Feng Li, Shilong Liu, Lei Zhang, Hang Su, Jun Zhu, Lionel M Ni, and Heung-Yeung Shum. Dino: Detr with improved denoising anchor boxes for end-to-end object detection. *arXiv preprint arXiv:2203.03605*, 2022. 1
- [48] Yinda Zhang and Thomas Funkhouser. Deep depth completion of a single rgb-d image. In *Proceedings of the IEEE Conference on Computer Vision and Pattern Recognition*, pages 175–185, 2018. 6